WORKSPACE COMPUTATION OF A TENSEGRITY-BASED PARALLEL MECHANISM

Zhifei JI[1], Min LIN[2], Chahua CHEN[3]

Tensegrity systems have advantages of light-weight, deployable and low inertia. They thus have been widely used in several disciplines such as architecture, aerospace, and mechanisms. In this work, a novel tensegrity-based parallel mechanism was proposed. Afterwards, the determination of the workspace of the mechanism was investigated. On the basis of the solutions to the inverse kinematic problem, a numerical method considering link length limitations, link interferences, joint angle limitations and energy constraints is presented to compute the workspace of the mechanism. This work lays the foundation for the design and application of tensegrity-based parallel mechanisms.

Keywords: Tensegrity; Workspace; Parallel mechanism; Energy constraints

List of symbols

$^{A}\boldsymbol{a}_i$: Coordinates of nodes A_i in the fixed reference frame A(X, Y, Z)

$^{A}\boldsymbol{b}_i$: Coordinates of nodes B_i in the fixed reference frame A(X, Y, Z)

K_i: Spring constant, L_i: Length of rod A_iB_i; U: Potential energy of the system

θ_{Amax}: The maximal allowable rotational angle of the spherical joints i

θ_{Bmax}: The maximal allowable rotational angle of the spherical joints j

1. Introduction

Tensegrity systems are formed by a combination of rigid elements (struts) under compression and elastic elements (cables or springs) under tension. The use of cables or springs as tensile components leads to an important reduction in the weight of the systems. Due to this attractive nature, tensegrity systems have been proposed to be used in many disciplines. Moreover, a detailed description of the history of tensegrity systems is provided in [1-2].

The first research work that deals with tensegrity systems was completed by Calladine [3]. Since then, tensegrity systems have been rapidly applied as structures in the architectural context. A tensegrity dome was proposed by

[1] Corresponding author. Lecturer, College of Mechanical and Energy Engineering, Jimei University, Xiamen 361021, China, e-mail: zfji18@163.com.

[2] Lecturer, College of Mechanical and Energy Engineering, Jimei University, Xiamen 361021, China, e-mail: linmin_0201@163.com

[3] Associate Professor, College of Mechanical and Energy Engineering, Jimei University, Xiamen 361021, China, e-mail: theodore@jmu.edu.cn.

Pellegrino [4]. Some design methods for tensegrity domes are proposed by Fu [5]. Afterwards, tensegrity structures have been also proposed to be served as bridges [6-9]. The use of cables or springs in tensegrities allows them to be deployable [10-11]. Due to this nature, some research works are found towards their use as antennas [12-13]. For static applications, the subject of form-finding of tensegrities has attracted the attention of several researchers [14-15]. Moreover, a review of form-finding methods was provided by Tibert and Pellegrino [16]. The basic issues about the statics of tensegrity structures were reviewed by Juan and Tur [17].

From an engineering point of view, tensegrities are a special class of structures whose components may simultaneously perform the purposes of structural force, actuation, sense and feedback control. For such kind of structures, pulleys or other kinds of actuators may stretch/shorten some of the constituting components in order to substantially change their forms with a little variation of the structure's energy. Therefore, tensegrity systems can be applied as mechanisms. Oppenheim and Williams [18] were the first to consider the actuation of tensegrity systems by modifying the lengths of their components in order to obtain tensegrity mechanisms. Afterwards, several mechanisms based on tensegrity systems were proposed, such as a flight simulator [19], a space telescope [20] and a tensegrity walking robot [21-23]. For tensegrity mechanisms, an interesting topic named tensegrity-based parallel mechanism has been proposed recently. The concept of tensegrity-based parallel mechanism was introduced by Marshall [24]. Then, Shekarforoush, Eghtesad and Farid [25] presented the statics of a 3-3 tensegrity-based parallel mechanism. Afterwards, Crane III, Bayat and Vikas [26] proposed a planar tensegirty-based parallel mechanism and completed its equilibrium analysis. Tensegrity systems have been identified as one of three main research trends in mechanisms and robotics for the second decade of the 21st century [27]. To the best of our knowledge, few researchers studied the workspace of special tensegrity-based parallel mechanisms considering the geometric and energy constraints.

In this paper, we studied the workspace of a 4-SPS tensegrity-based parallel mechanism. The main contribution of this article is twofold. First, on the basis of the solutions to the inverse kinematic problems, we proposed a method considering link length limitations, link interferences, joint angle limitations and energy constraints to compute the mechanism's workspace. Second, the volume of the workspace along with the mechanism's geometric parameters is researched.

This paper is organized as follows. First, the architecture of the 4-SPS tensegrity parallel mechanism are presented in section 2. Secondly, the proposed discretization approach for computing the equilibrium workspace is illustrated in detail in section 3. Third, based on an equilibrium workspace criterion, effects of different geometric parameters and constraints on the equilibrium workspace are

examined in section 4. The numerical example is simulated in section 5. Finally, conclusion and the future work are reported in section 6.

2. Mechanism description

A diagram of the 4-SPS tensegrity parallel mechanism is shown in Fig. 1. It consists of a square top platform $B_1B_2B_3B_4$, a square base platform $A_1A_2A_3A_4$, four springs and four struts. The struts are joining node pairs A_iB_i (i=1, 2, 3, 4) while the springs are joining node pairs A_iB_{i+1} (i=1, 2, 3, 4 with i+1=1 if i = 4). From Fig. 1, it can be seen that the sides of the square platform formed by nodes $A_1A_2A_3A_4$ and $B_1B_2B_3B_4$ have the length 2a and 2b, respectively. Moreover, the length of the prismatic actuators joining node pairs A_iB_i is denoted by L_i. It is assumed that the springs are linear with stiffness K_j and lengths l_j (j = 1, 2, 3, 4). These springs are also assumed to have the same free length L_0. The stiffnesses of the struts are considered to be infinite relative to those of the springs.

As illustrated in Fig. 1, a fixed reference frame A(X, Y, Z) is located at the center of the square $A_1A_2A_3A_4$ with its X axis parallel to the line joining nodes A_3 and A_4 and its Z axis perpendicular to the base platform $A_1A_2A_3A_4$, while a moving reference frame B(X_1, Y_1, Z_1) is located at the center of the top platform $B_1B_2B_3B_4$ with its X axis parallel to the line joining nodes B_3 and B_4 and its Z_1 axis perpendicular to the top platform $B_1B_2B_3B_4$. Moreover, the vectors specifying the positions of nodes A_i and B_i in the fixed reference frame are defined as ${}^A\boldsymbol{a}_i$ and ${}^A\boldsymbol{b}_i$, respectively. Also, the vectors specifying the positions of nodes B_i in the moving reference frame are defined as ${}^B\boldsymbol{b}_i$.

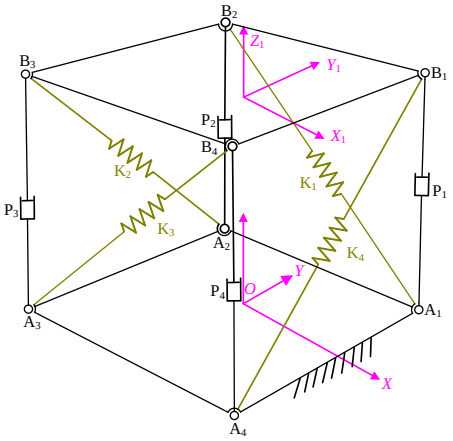

Fig. 1. 4-SPS tensegrity parallel mechanism

In Fig. 1, the vectors specifying the positions of nodes A_i in the fixed reference frame can be easily derived.

$$ {}^{A}\boldsymbol{a}_1 = \begin{bmatrix} a \\ a \\ 0 \end{bmatrix}, {}^{A}\boldsymbol{a}_2 = \begin{bmatrix} -a \\ a \\ 0 \end{bmatrix}, {}^{A}\boldsymbol{a}_3 = \begin{bmatrix} -a \\ -a \\ 0 \end{bmatrix}, {}^{A}\boldsymbol{a}_4 = \begin{bmatrix} a \\ -a \\ 0 \end{bmatrix} \tag{1} $$

Similarly, the vectors specifying the positions of nodes B_i in the moving reference frame can be easily derived.

$$ {}^{B}\boldsymbol{b}_1 = \begin{bmatrix} b \\ b \\ 0 \end{bmatrix}, {}^{B}\boldsymbol{b}_2 = \begin{bmatrix} -b \\ b \\ 0 \end{bmatrix}, {}^{B}\boldsymbol{b}_3 = \begin{bmatrix} -b \\ -b \\ 0 \end{bmatrix}, {}^{B}\boldsymbol{b}_4 = \begin{bmatrix} b \\ -b \\ 0 \end{bmatrix} \tag{2} $$

Furthermore, the position and orientation of the top platform $B_1B_2B_3B_4$ are described by the position vector $\boldsymbol{P} = [x, y, z]^T$ and the rotation matrix $\boldsymbol{T}$ with respect to the fixed reference frame. From Fig. 1, it can be seen that the rotation matrix $\boldsymbol{T}$ can be defined by rotating the moving reference frame γ about Z_1 axis and followed β about Y_1 axis, α about X_1 axis. $\boldsymbol{T}$ thus takes the following form.

$$ \boldsymbol{T} = \begin{bmatrix} c\beta c\gamma & s\alpha s\beta c\gamma - c\alpha s\gamma & s\alpha s\gamma + c\alpha s\beta c\gamma \\ c\beta s\gamma & c\alpha c\gamma + s\alpha s\gamma & c\alpha s\beta s\gamma - s\beta c\gamma \\ -s\beta & s\alpha c\beta & c\alpha c\beta \end{bmatrix} \tag{3} $$

where s and c are used to represent the sine and cosine function, respectively. The position vectors of points B_i (i=1, 2, 3, 4) with respect to the fixed reference frame can be obtained:

$$ {}^{A}\boldsymbol{b}_i = \boldsymbol{P} + \boldsymbol{T} \cdot {}^{B}\boldsymbol{b}_i, \ i = 1, \ 2, \ 3, \ 4 \tag{4} $$

Considering the conditions that the potential energy will reach its minimum when the mechanism is in equilibrium, the position and orientation of the top platform can be determined by fixing the actuator lengths L_i. For this reason, it is appropriate to say that the mechanism has four degrees of freedom when it is in equilibrium.

Therefore, the system's output vector can be chosen as $\boldsymbol{O} = [x, y, z, \alpha]^T$ while its input vector is chosen as $\boldsymbol{I} = [L_1, L_2, L_3, L_4]^T$. With the position vectors of points A_i and B_i now known, the vector of the ith link can be written as

$$ L_i = {}^{A}\boldsymbol{b}_i - {}^{A}\boldsymbol{a}_i, \ i = 1, \ 2, \ 3, \ 4 \tag{5} $$

Similarly, the length of the ith spring can be given as

$$ \boldsymbol{l}_i = \left| {}^{A}\boldsymbol{b}_{i+1} - {}^{A}\boldsymbol{a}_i \right|, \ (i = 1, \ 2, \ 3, \ 4; \ i+1 = 1 \text{ when } i = 4) \tag{6} $$

Then the potential energy of the mechanism can be obtained.

$$U = \frac{1}{2}\sum_{i=1}^{4} K_i \left(l_i - L_0\right)^2 \tag{7}$$

3. Workspace computation

The workspace of a mechanism is defined as the region that its end-effector can reach and is generally considered to be an important performance indicator. For the mechanism shown in Fig. 1, its workspace can be considered as the range of the output variables *x*, *y*, *z* and *a*. Unlike in conventional mechanisms, the workspace of the 4-SPS tensegrity-based parallel mechanism depends not only on the geometric constraints but also on the energy constraints.

The geometric constraints of the mechanism include link length limitations, link interferences and joint angle constraints.

3.1 Link length limitations

The link length limitations corresponds to the ranges that the prismatic actuators can operate, which are given by

$$L_{i\min} \le L_i \le L_{i\max} \tag{8}$$

where $L_{i\min}$ and $L_{i\max}$ are the minimal and maximal allowable length of link *i*, respectively.

It is noted that if one of link length is at its extreme value, the workspace will reach its boundaries.

3.2 Link interference

Bars' interference might occur in the real world due to the fact that bars have physical dimensions. It is supposed that the bars are cylindrical with a diameter *D*. Then, the shortest distance between the center lines of two adjacent bars is denoted by D_i (i = 1, 2, 3). When two bars do not interfere, the following conditions should be satisfied.

$$D_i \ge D \tag{9}$$

In a previous work [28], the computation of D_i have been discussed explicitly. The method for computing D_i is employed in this paper to establish the equations corresponding to bars' interference. Due to space limitation, this procedure will not be detailed here.

3.3 Joint angle constraints

The links are typically attached to the top and base platforms by spherical joints. Generally, a spherical joint is free to rotate about all three axes. However, in practice, its motion is restricted by the physical construction of the joints. As shown in Fig. 2, the rotational angle of a ball joint, θ, defined as the angle between the Z-axis of a coordinate system attached to its socket, and $\boldsymbol{u}$, a vector along the leg connected to the joint, is physically constrained. It can be observed that every practical joint has its maximal rotational angle value θ_{max}.

It is assumed that the socket of a spherical joint i connecting the base and the link is installed so that a unit vector $\boldsymbol{n}_{Ai}$ describes its orientation with respect to the base coordinate system. As shown in Fig. 3, the rotational angle of the ball joint and its constraint can be computed by:

$$\theta_{Ai} = \arccos\left(\frac{\boldsymbol{l}_i \cdot \boldsymbol{n}_{Ai}}{|\boldsymbol{l}_i|}\right) \le \theta_{A\max} \tag{10}$$

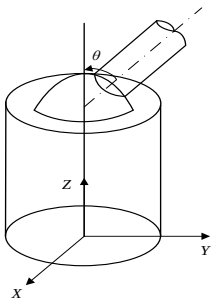

Fig. 2 Ball joint rotational angle

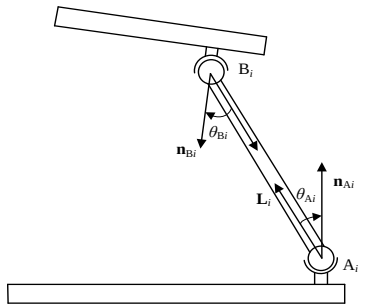

Fig. 3 Joint rotational constraints

Similarly, for the rotational angle of the spherical joint j connecting the top platform and the joint angle constraint can be expressed by:

$$\theta_{Bj} = \arccos\left(\frac{\boldsymbol{l}_j \cdot \boldsymbol{T}\boldsymbol{n}_{Bj}}{|\boldsymbol{l}_j|}\right) \le \theta_{B\max} \tag{11}$$

where $\boldsymbol{n}_{Bi}$ is the unit vector which describes the spherical joint orientation with respect the moving coordinate system, and θ_{Amax} and θ_{Bmax} are the maximal allowable rotational angles of the spherical joints i and j, respectively.

3.4 Energy constraints

For tensegrity-based parallel mechanisms, the workspace should consider the mechanism's energy constraints introduced by the conditions that the potential

energy is always at its minimum when the mechanism is in equilibrium. From Eq. (7), the energy constraints equations can be expressed by

$$\begin{aligned} \frac{\partial U}{\partial \beta} &= 0 \\ \frac{\partial U}{\partial \gamma} &= 0 \end{aligned} \tag{12}$$

3.5 Determination of the workspace

In this section, an algorithm is proposed for determining the equilibrium workspace regions of the tensegrity-based parallel mechanism. For a given output variables $\boldsymbol{O_0} = [x_0, y_0, z_0, \alpha_0]^T$, the variables β_0 and γ_0 can be computed by Eq. (12). With the variables x_0, y_0, z_0, α_0, β_0 and γ_0 known, the coordinates of nodes A_{i0} and B_{i0} can be determined using Eqs. (1) and (4). Afterwards, the length l_{i0}(see section 3.1), minimal distances between links D_{i0} (see section 3.2) and the rotational angle variables θ_{Ai0} and θ_{Bj0} (see section 3.3) can be computed. It is noted that if the point corresponding to $\boldsymbol{O_0} = [x_0, y_0, z_0, \alpha_0]^T$ belongs to the mechanism's workspace, the following equation should be satisfied.

$$\begin{aligned} & L_{\min} \le l_{i0} \le L_{\max} \\ & D_{i0} \ge D \\ & \theta_{Ai0} \le \theta_{A\max} \\ & \theta_{Bi0} \le \theta_{B\max} \end{aligned} \tag{13}$$

The procedure for computing the workspace for a given orientation of the tensegrity mechanism is given in Fig. 4.

The volume of the workspace can be used as a criterion for workspace evaluation and optimization. The equilibrium workspace volume is a function of the geometric parameters as well as the constraints of the system. Therefore, the volume criterion can also be used to evaluate the effect of different geometric parameters and constraints on the workspace.

In this paper, the volume of the equilibrium workspace of 4-SPS can be computed as

$$V = \Delta x \cdot \Delta y \cdot \Delta z \cdot length(x) \tag{14}$$

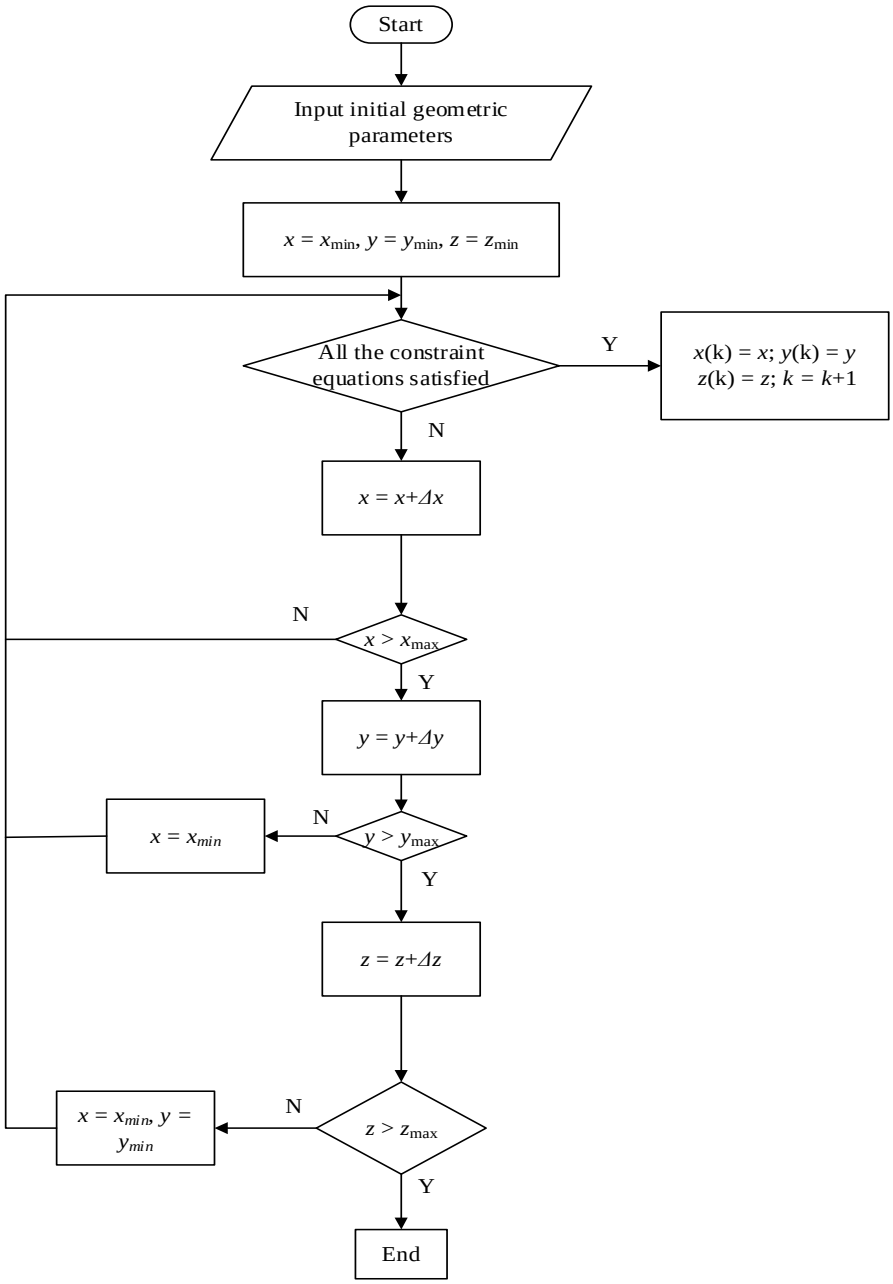

Fig. 4 Procedure for determination the equilibrium workspace of tensegrity mechanism

4 Numerical simulations

In order to validate the approach to computing the equilibrium workspace of tensegrity-based parallel mechanism in the previous section, a numerical example is provided.

The mechanism's parameters are given in the following.

- a = 1, b = 0.5, L_{min} = 0.5, L_{max} = 3, θ_{max} =70°, D = 0.015,
- $\Delta x = \Delta y = \Delta z = \Delta\alpha = \Delta\beta = \Delta\gamma = 0.05$,
- $x \in$[-1.5, 1.5], $y \in$ [-1.5, 1.5], $z \in$ [0.5, 2.5], $\beta \in$ [-π/2, π/2], $\gamma \in$ [-π/2, π/2],
- α = -0.1708, ε = 0.05.

The workspace of the tensegrity-based parallel mechanism is shown in Fig. 5. From Fig. 5, it can be seen that the workspace is symmetrical with the x-axis and y-axis, respectively.

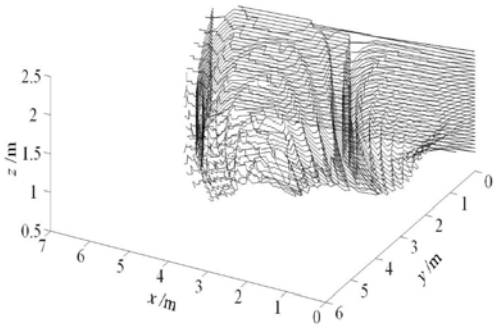

Fig. 5. Workspace of the mechanism

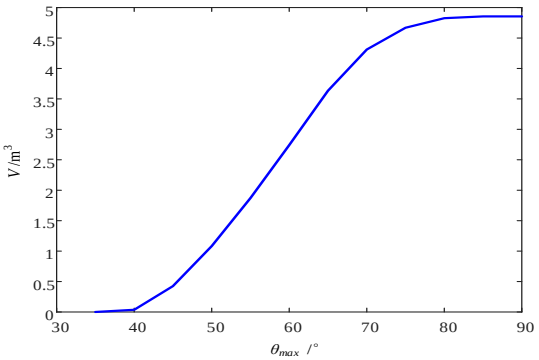

Fig.6. The evolution of the volume V along with the maximal rotational angle θ_{max}

The evolution of the volume of the mechanism's workspace along with the maximal rotational angle θ_{max} is shown in Fig. 6. From Fig.6, it can be seen that the workspace volume increase with θ_{max}.

Let k be the ratio of a and b, the evolution of the volume of the mechanism's workspace along with the parameter k can be obtained, which is shown in Fig. 7. From Fig. 7, it can be seen that the workspace volume reach the maximum when k=0.3, and the workspace volume increase with k when $k < 0.3$, and the workspace volume decrease with an increase in k when $k > 0.3$. This law need to be considered when the mechanism is put to use.

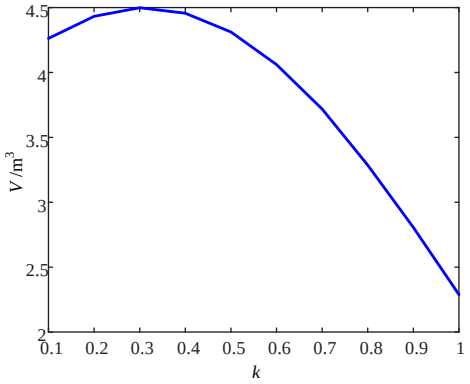

Fig. 7. The evolution of the volume V along with the parameter k

5 Conclusion

A numerical approach for determining the workspace of a 4-SPS tensegrity-based parallel mechanism has been proposed based on the inverse kinematics of the mechanism. Then, the workspace volume has been computed. The evolutions of the workspace volume along with the maximal rotational angle and the parameter k have been investigated respectively. The results indicates that the workspace volume reach the maximum when $k = 0.3$, and it increases with k when $k < 0.3$. Moreover, the workspace volume decreases with an increase in the parameter k when $k > 0.3$. The obtained laws can be used for optimizing workspace and designing the parameters of such mechanisms. While the numerical method for computing the workspace proposed in this paper can be extended in a straightforward manner to other tensegrity-based mechanisms.

Acknowledgment

This research is supported by the Natural Science Foundation of Fujian Province, China (No. 2017J05084) and the Science Foundation of Jimei University, China (No. ZQ2017005).

R E F E R E N C E S

[1]. *R. Motro*, Tensegrity: structural systems for the future, Kogen Page Science, Guildford, 2003.
[2]. *R. E. Skelton and M. C. Oliveira*, Tensegrity Systems, Springer, New York, 2009.
[3]. *C. R. Calladine*, "Buckminster Fuller's "tensegrity" structures and Clerk Maxwell's rules for the construction of stiff frames", International Journal of Solids and Structures, vol**. 14**, no. 2, 1978, pp. 161-172.
[4]. *S. Pellegrino*, "A class of tensegrity domes", International Journal of Space Structures, vol. **7**, no. 2, 1992, pp. 127-142.
[5]. *F. Fu*, "Structural behavior and design methods of tensegrity domes", Journal of Constructional Steel Research, vol. 61, no. 1, 2005, pp. 23-35.

[6]. *L. Rhode-Barbarigos, N. B. H. Ali, R. Motro, et al.*, "Designing tensegrity modules for pedestrian bridges", Engineering Structures, vol. **32,** no. 4, 2010, pp. 1158-1167.
[7]. *L. Rhode-Barbarigos, N. B. H. Ali, R. Motro, et al*., "Design aspects of a deployable tensegrity -hollow-rope footbridge", International Journal of Space Structures, vol. **27,** no. 2-3, 2012, pp. 81-96.
[8]. *S. Korkmaz, N. B. H. Ali and I. F. C. Smith*, "Configuration of control system for damage tolerance of a tensegrity bridge", Advanced Engineering Informatics, vol. **26**, no. 1, 2012, pp. 145-155.
[9]. *R. E. Skelton, F. Fraternali, G. Carpentieri, et al.*, "Minimum mass design of tensegrity bridges with parametric architecture and multiscale complexity", Mechanics Research Communications, vol. 58, 2014, pp. 124-132.
[10]. *J. Duffy, J. Rooney, B. Knight, et al.*, "Review of a family of self-deploying tensegrity structures with elastic ties", Shock and Vibration Digest, vol. **32,** no. 2, 2000, pp. 100-106.
[11]. *H. Furuya*, "Concept of deployable tensegrity structures in space applications", *International Journal of Space Structures*, vol**. 7,** no. 2, 1992, pp. 143-152.
[12]. *G. Tibert*, Deployable tensegrity structures in space applications. PhD Thesis, Royal Institute of Technology, Sweden, 2002.
[13]. *N. Fazli and A. Albedian*, "Design of tensegrity structures for supporting deployable mesh antennas", Scientia Iranica, vol. **18**, no. 5, 2011, pp. 1078-1087.
[14]. *N. Vassart and R. Motro*, "Multiparametered form finding method: application to tensegrity systems", International Journal of Space Structures, vol. 14, no. 2, 1992, pp. 147-154.
[15]. *K. Koohestani*, "Form-finding of tensegrity structures via genetic algorithm", *International Journal of Space Structures*, vol**. 49**, no. 5, 2012, pp. 739-747.
[16]. *A. Tibert and S. Pellegrino*, "Review of form-finding methods for tensegrity structures", International Journal of Space Structures, vol. 18, pp. 4, 2003, pp. 209-223.
[17]. *S. H. Juan, and J. M. M. Tur*, "Tensegrity frameworks: static analysis review", *Mechanism and Machine Theory*, vol. **43**, no. 7, 2008, pp. 859-881.
[18]. *I. J. Oppenheim and W. O. Williams*, "Tensegrity prisms as adaptive structures. in: Proceedings of the 1997 ASME International Mechanical Engineering Congress and Exposition, Dallas, USA, 1997.
[19]. *C. Sultan and M. Corless*, "Tensegrity flight simulator", Journal of Guidance, Control, and Dynamics, vol**. 23**, no. 6, 2000, pp. 1055-1064.
[20]. *C. Sultan, M. Corless and R. E. Skelton*, "Peak to peak control of an adaptive tensegrity space telescope", in: Proceedings of SPIE-The International Society for Optical Engineering, Newport Beach, USA, 1999.
[21]. *C. Paul, H. Lipson and F. Valero-Cuevas*, "Design and control of tensegrity robots for locomotion", IEEE Transactions on Robotics, vol. 22, no. 5, 2006, pp. 944-957.
[22]. *A. G. Rovira and J. M. M. Tur*, "Control and simulation of a tensegrity-based mobile robot", *Robotics and Autonomous Systems*, vol. **57**, no. 5, 2009, pp. 526-535.
[23]. *S. Hirai and R. Imuta*, "Dynamic simulation of six-strut tensegrity rolling", in: Proceedings of the 2012 IEEE International Conference on Robotics and Biomimetics, Guangzhou, China, 2012.
[24]. *M. Q. Marshall*, Analysis of tensegrity-based parallel platform devices. Master's Thesis, University of Florida, Florida, 2003.
[25]. *S. M. M. Shekarforoush, M. Eghtesad and M. Farid*, "Kinematic and static analyses of statically balanced spatial tensegrity mechanism with active compliant components", *Journal of Intelligent & Robotic Systems*, vol**. 71**, no. 3-4, 2013, pp. 287-302.

[26]. *C. D. Crane III, J. Bayat, V. Vikas, et al*., "Kinematic analysis of a planar tensegrity mechanism with pre-stressed springs", In Advances in Robot Kinematics: Analysis and Design, 2003, pp. 419-427, 2003.
[27]. *J. M. McCarthy*, "21st century kinematics: Synthesis, compliance and tensegrity", Journal of Mechanisms and Robotics, vol. **3**, no. 2, 2011, pp. 020201-020201.
[28]. *M. Lin, T. Li, Z. Ji, M. Che*, "Force-displacement relationships of a tensegrity structure considering bar interference", UPB Scientific Bulletin, Series D: Mechanical Engineering, vol. **78**, no. 2, 2016, pp. 1-16.